JOURNAL OF MATERIALS SCIENCE, 30 (1995) 5495–5501

Microstructure and mechanical properties relations for green bodies compacted from spray dried granules

D. C. C. LAM
Department of Mechanical Engineering, Hong Kong University of Science and Technology, Clear Water Bay, Kowloon, Hong Kong

K. KUSAKARI
Inorganic Materials Section, The 3rd Materials Department, Hitachi Research Laboratory, 1-1 Saiwai-cho, 3-chome, Hitachi-shi, Ibaraki-ken 317 Japan

Alumina granules from three binder systems were spray dried and pressed into bars at varied pressure. Granules are classified as strong, medium and weak as to reflect the different amount of poly(vinyl-butyral) binder and liquid paraffin plasticizer used in the binder system. Mechanical properties of the pressed bars were obtained from a four-point bend test and microstructures were examined using scanning electron microscopy SEM. Strengths and fracture toughnesses are found to increase as a function of compaction pressure, while the calculated effective flaw size is independent of the compaction pressure for all three granule types. Microstructural examination of fracture surfaces revealed that samples compacted at high pressure exhibited more transgranular fracture than samples compacted at low pressure. Evidently, higher pressure had increased the intergranular fracture resistance which correspondingly increased the fracture toughness of the pressed bars. For bars pressed from granules, green body strengths and toughnesses are strongly dependent on the cohesion between pressed granules and not on the effective processing flaw size.

1. Introduction

Among the many forming processes available in the production of ceramic articles, compaction from granules is becoming increasingly popular in commercial production [1] because of its reproducibility and high production rate. To increase reliability, higher green strengths are generally desired to minimize handling and processing damage. A cost-effective method to increase green strength is to increase the forming pressure. At high forming pressure, the contact area between pressed granules are increased such that the size of intergranular voids which can act as flaws are reduced. In this paper, the effect of compaction pressure on the mechanical properties and on the microstructures are examined for three sets of spray dried alumina granules. The relation between the binder systems, compaction pressure, strength and microstructure, and in particular, the microstructural origin of the increased strength at higher forming pressure are discussed.

2. Experiments

To determine the effect of binder system and compaction pressure on the mechanical properties of compacted bars, three different alumina granules were made by spray drying 0.2 μm α-alumina (Sumitomo AKP-20) with three different combinations of binder and plasticizer. Measured quantities of high molecular weight organic (in the proportions listed in Table I) sufficient for 500 ml of final slurry volume were mixed in ethanol and ultrasonicated for 15 min. Alumina powders (either 28 vol % or 32 vol % of the final slurry volume) were slowly stirred into the prepared ethanol solution and ultrasonicated for 20 min to homogenize and disperse the powder. Then the slurry was magnetically stirred for 2 h and ultrasonicated once more for 20 min before spray drying. Spray drying was done in a small Tokyo Rikakikei SD-2 spray dryer equipped with an air pressured spraying nozzle at an inlet temperature of 75 °C, outlet temperature of 50 °C and spraying pressure of 1.38 kPa. After spray drying, the granules were collected in a double capped plastic bottle for storage.

Granules for all three systems were similar such that only the micrograph for the medium case are presented in Fig. 1. From these granules, 2 g of granules were weighed, poured into a double action stainless tool steel die and uniaxially pressed in a Riken Seiki model

0022–2461

TABLE I Percentages of organic solvents used.

Alumina granule[a]	PVB mass%	LP mass%	PEI mass%	Solid loading%
strong	3	0	0.25	32 vol
medium	2	0	0.25	32 vol
weak	1	1	0.25	28 vol

PVB Polyvinyl butyral MW = 35 000; PEI polyethylene imine MW = 70 000; LP liquid paraffin.
Mass% based on solid alumina weight.
[a]The granules are classified according to green strength (Fig. 4).

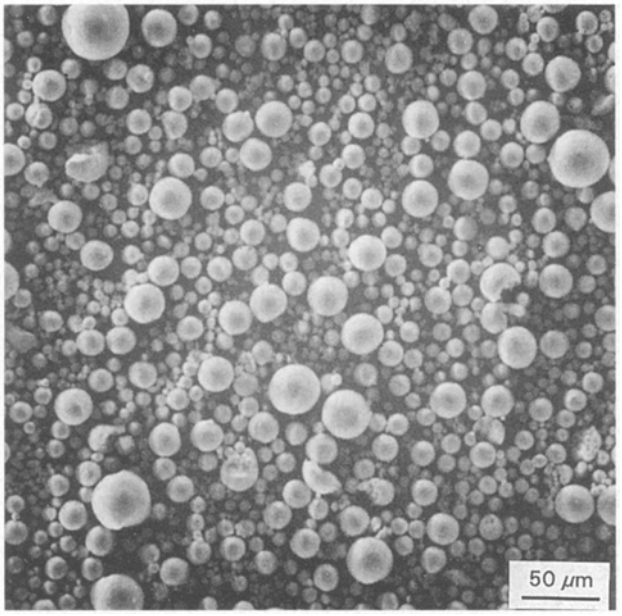

Figure 1 SEM micrograph of a representative spray dried granule from the medium granules. Granules from hard and soft are similar in size and shape.

R-213 desk top press at pressures between 100 to 400 MPa at 50 MPa intervals. Die wall lubrication was not used because lubricant itself may be incorporated into the body as inclusion flaws. Prismatic bars 50 × 5 mm with thicknesses varying from 3.1 to 3.5 mm were produced. A minimum of two bars at each compaction pressure and for each binder system totalling more than 45 bars were produced for green strength testing. After pressing, the bars were equilibrated in a dessicator at atmospheric pressure for over 24 h. Then corners and edges were hand beveled and the bars' opposite surfaces were paralleled on 3 μm lapping tape. Strength tests were done in a SiC four-point bending jig with an inner span of 10 mm and an outer span of 30 mm. The jig loaded with bar was tested in a screw driven test frame at a cross-head displacement rate of 20 μm min^{-1}. The test load was measured using a 500 kg-load cell set at a 5 kg scale having a resolution of 0.2% of scale. After green strength testing, the organics in the bars were pyrolysed away by heating the broken bars from room temperature at a ramp rate of 50 °C h^{-1} to 800 °C and held for 2 h before cooling down at 200 °C h^{-1} to 300 °C and then furnace cooled to room temperature. The calcined bars' densities were measured using Archimedes' method with 1-propanol (0.798 g cm^{-3} at 20 °C) as the immersion liquid. From dimensional measurements, dimensional changes from the green state to the calcined state were negligible such that the calcined densities were taken to be the same as the ceramic solid densities for the green bars.

3. Data Analysis

Representative load-displacement curves for all three binder systems are plotted in Fig. 2. The load deflection curves are generally non-linear such that conventional linear elastic relation [2] for strength σ_f from a four-point bending test

$$\sigma_f = 3P\frac{l}{bh^2} \quad (1)$$

(l is the inner span length, 1/3 of the outer span, b is the width, h is the bar thickness and P is the peak load) cannot be used. An alternate relation accounting for the nonlinear behaviour must be used.

For pure bending with antisymmetric tensile and compressive bending strains in the bar, classical bending theory [2] gives the fundamental relation between the peak load P and the bar's stress–strain state and dimensions as

$$P = \frac{bh^2}{l\varepsilon_f^2}\int_0^{\varepsilon_f}\sigma\varepsilon d\varepsilon \quad (2)$$

where ε_f is the surface strain on the tensile surface of the bar and the integral is taken from the neutral plane to the bar surface. Approximating the non-linear stress–strain behaviour as a polynomial stress–strain relation

$$\sigma = K_1\varepsilon + K_2\varepsilon^2 \quad (3)$$

Equation 2 can be rewritten by substituting Equation 3 into Equation 2. Simplification gives

$$P_f = \frac{bh^2}{l}\left(\frac{K_1}{3}\varepsilon_f + \frac{K_2}{4}\varepsilon_f^2\right) \quad (4)$$

For four-point bending, the surface tensile strain ε_f is related to the cross-head displacement δ_f through [3]

$$\varepsilon_f = \frac{3h}{5l^2}\delta_f \quad (5)$$

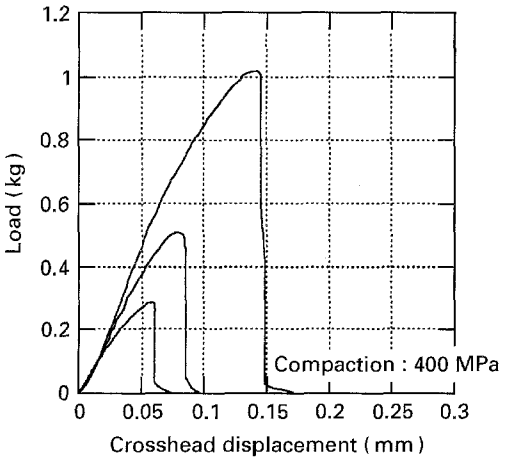

Figure 2 Four-point bending load–cross-head displacement curves for strong (top), medium (middle) and weak (bottom) granules pressed at 400 MPa. Cross-head speed is at 20 μm min^{-1} with loading points symmetrically separated at 10 mm apart.

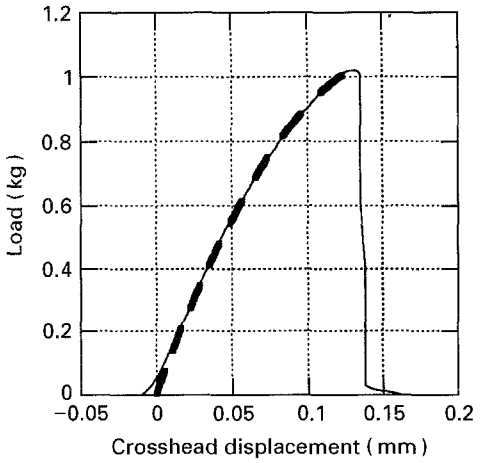

Figure 3 Two-term polynomial curve fit for load–cross-head displacement curve of bars pressed at 400 MPa from strong granules. The coefficients from the curve fit ($y = 13x - 40x^2$) together with the peak load are used to calculate the fracture stress.

which when combined with Equation 4 gives

$$P_f = H_1\delta_f + H_2\delta_f^2 \tag{6}$$

where

$$H_1 = \frac{bh^3}{5l^3}K_1 \tag{7a}$$

and

$$H_2 = \frac{9bh^4}{100l^5}K_2 \tag{7b}$$

In this study, the constants were obtained directly by mathematically fitting Equation 6 to the experimental load–displacement curve. To assure that the peak load was properly accounted for, the peak load was fully weighed to assure that the curve fit passes through the peak load. A typical curve fit and its fitted constants are shown in Fig. 3 for the case of strong granules pressed at 400 MPa. As can be seen from the curve fit, the initial loading non-linearity associated with load point deformation was ignored. From the constants and the peak load, the fracture strain and fracture strength were calculated from Equations 4 and 3, respectively.

In addition to the fracture strength, the fracture behaviour of the compliant green bars was typically non-catastrophic such that the energy as represented by the area under the load–displacement curve can be equated to the work done to fracture the bar. J_{IC}, the work of fracture per unit cross-sectional area for non-linear material was obtained by integrating the load–displacement curve and dividing by the cross-sectional fractured area of the bar. Combined with the elastic modulus calculated from the linear portion of the curve using the relation [3]

$$E = \frac{5l^3}{3bh^3}\frac{(P_2 - P_1)}{(\delta_2 - \delta_1)} \tag{8}$$

the fracture toughness K_{IC} can be obtained using [4].

$$K_{IC} = \sqrt{EJ_{IC}} \tag{9}$$

4. Results and Discussion

Strength as a function of the compaction pressure and relative solid density were plotted in Figs 4 and 5. As expected, strengths of bars pressed from granules were dependent on the binder system as well as the compaction (uniaxial pressing) pressure. The elastic modulus, the fracture energy and the fracture toughness were plotted respectively in Figs 6, 7 and 8. Data indicated that all three parameters increased with increasing relative density. The rate of increase is highest for bars pressed from strong granules and lowest for weak granules. In addition, an effective flaw size c was calculated from the rearranged Griffith's relation

$$c = \left(Y\frac{K_{IC}}{\sigma_c}\right)^2 \tag{10}$$

The stress concentration factor Y was taken as 1 since the shapes of flaws were not known. The plot of effective flaw size as a function of compaction pressure (Fig. 9) indicated that higher pressure did not affect the effective flaw size. A cross plot of strength versus fracture toughness showing this trend is shown in Fig. 10. The increased strengths at higher compaction pressure appear to be primarily dependent on higher fracture

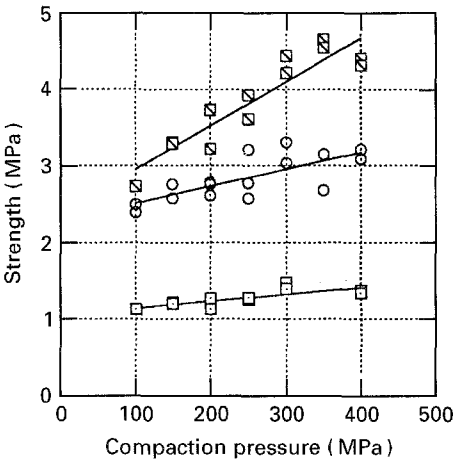

Figure 4 Strength versus compaction pressure for hard (▨), medium(○) and soft (□) granules.

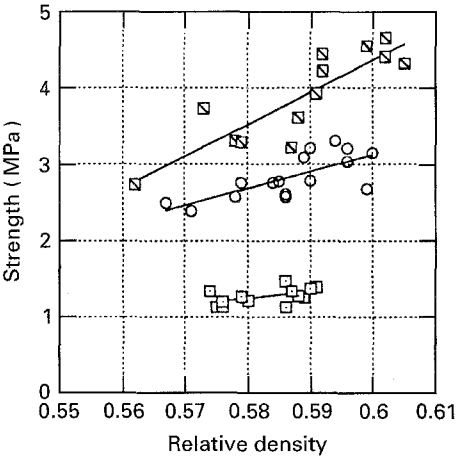

Figure 5 Strength versus relative density for strong (▨), medium (○) and weak (□) granules.

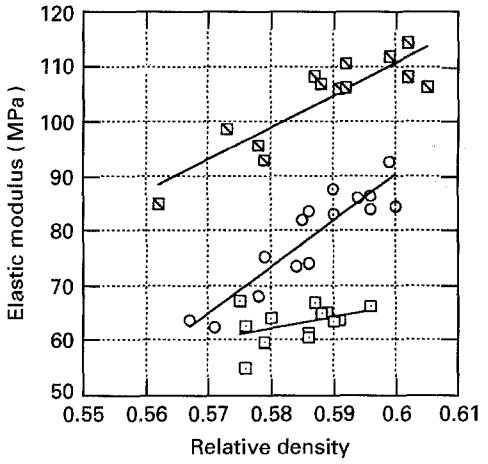

Figure 6 Elastic modulus versus relative density for strong (▨), medium (○) and weak (□) granules.

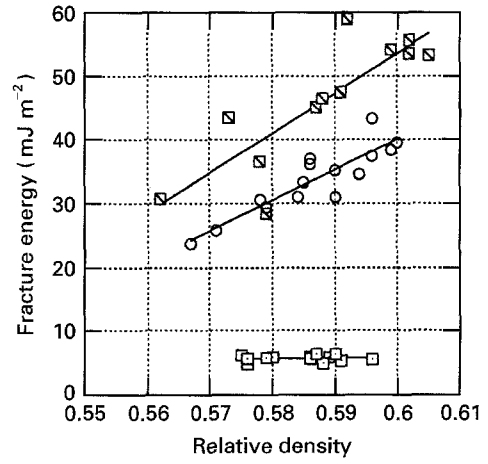

Figure 7 Fracture energy versus relative density for strong (▨), medium (○) and weak (□) granules.

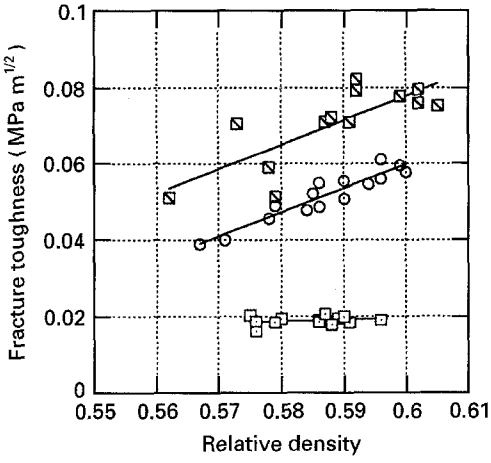

Figure 8 Fracture toughness versus relative density for strong (▨), medium (○) and weak (□) granules.

toughness resulting from increased compaction pressure.

The effect of pressure on green strength has been investigated in the field of powder metallurgy [5–8]. The strength of green bars compacted from metal powders had been known to increase as a function of compaction pressure. The strengthening mechanism had been attributed to both geometric interlocking

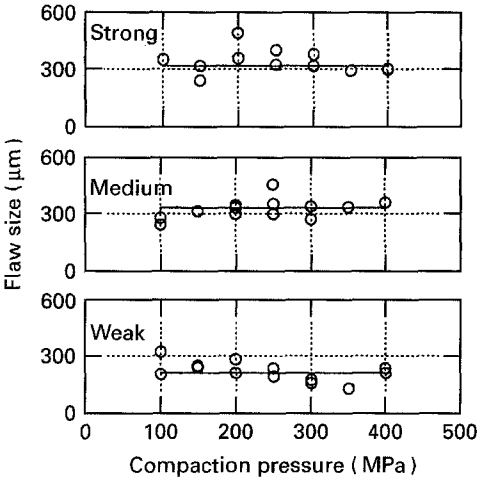

Figure 9 Effective flaw size versus compaction pressure for strong granules (top), medium granules (middle) and weak granules (bottom). The median effective flaw size is about 310 μm (horizontal line) for both strong and medium granules while the case for weak granules is about 220 μm.

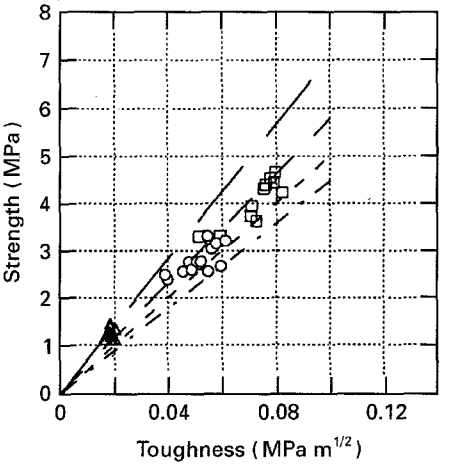

Figure 10 Strength versus fracture toughness for strong (□), medium (○) and weak (△) granules. —— $c = 200\,\mu m$; – – $c = 300\,\mu m$; ---- $c = 400\,\mu m$; – · – · $c = 500\,\mu m$.

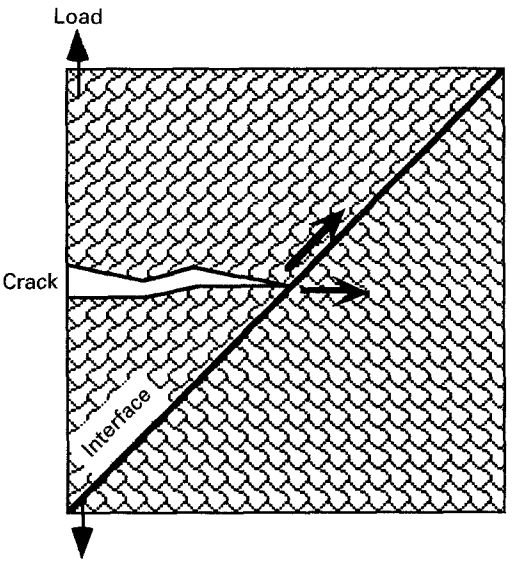

Figure 11 Schematic of crack path selection at material interface. The crack would kink and propagate along interface when interface is weak, but would remain along the principal stress direction and propagate transgranularly if the interface is strong.

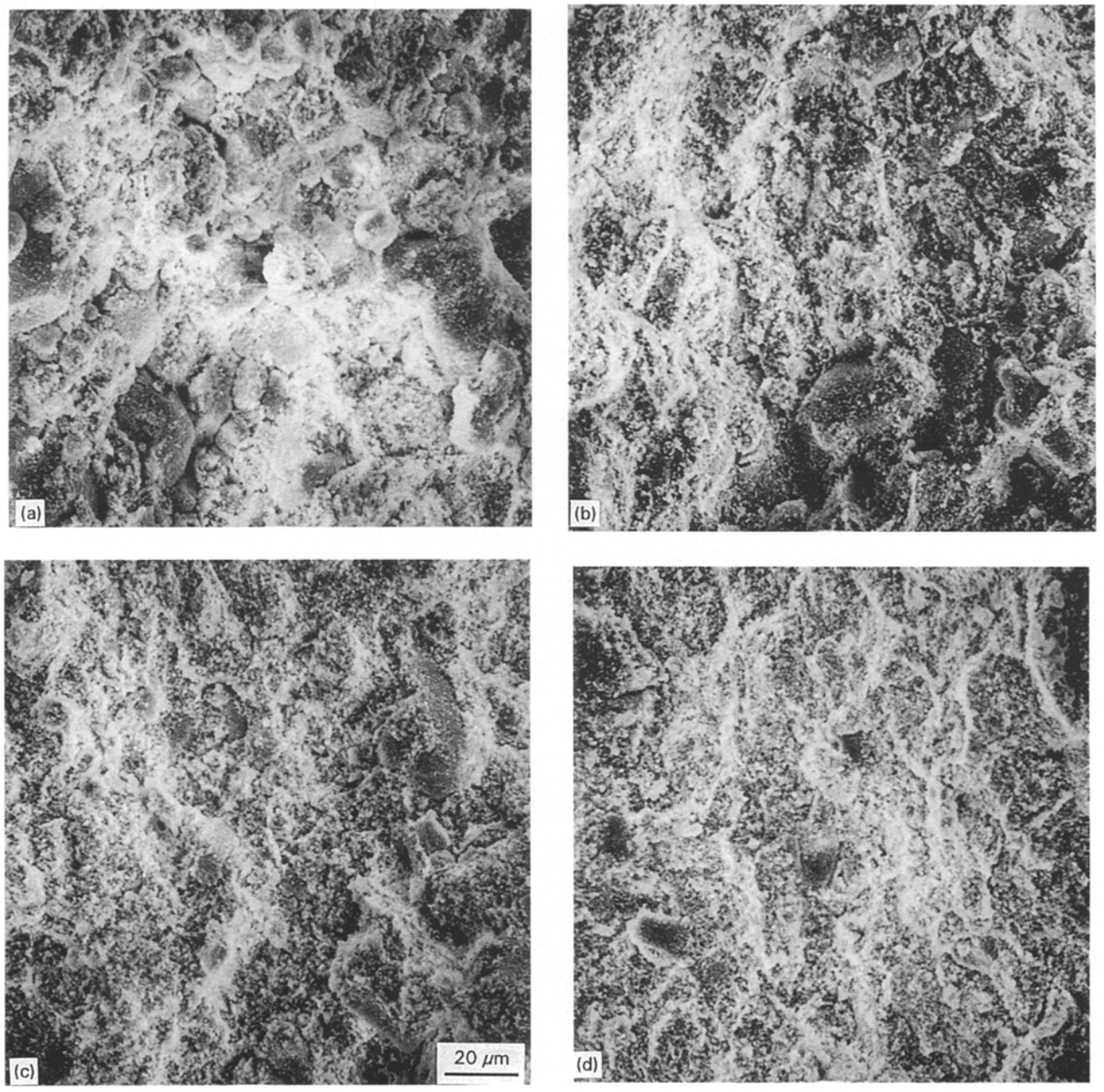

Figure 12 SEM fracture surface of strong granules compacted at (a) 100 MPa; (b) 200 MPa; (c) 300 MPa; and (d) 400 MPa. Fracture surface becomes increasingly transgranular as compaction pressure increases.

and improved cohesion between granules (cold welding). Interlocking is the primary strengthening mechanism for irregular particles, particularly at low compaction pressure where cold welding is not active. For compacts made from regularly shaped particles, interlocking mechanism is a minor contributor to the strengthening [7, 8]. Green strengths of compacts pressed from regularly shaped metal powders appear to be associated primarily with intergranular cohesion. The increase in strength as a function of compaction pressure observed in this study is most likely related to improved interfacial granular cohesion.

The effect of interfacial toughness on crack propagation had been studied in composite fracture mechanics [9,10]. Consider the case of a bimaterial interface which is inclined at 45 ° to a propagating horizontal crack (Fig. 11), the crack can either kink and propagate along the weaker interface or continue to propagate across the material along the direction with the highest principal opening tensile stress. The choice between intergranular fracture and transgranular fracture depends on the elastic mismatch between the materials on both sides of the interface and on the ratio of intergranular fracture energy to transgranular fracture energy [9,10]. For the case of a crack propagating in a bar pressed from granules, the materials on either side of the granular interface are the same and there is no elastic mismatch. The choice between intergranular and transgranular fracture depends mainly on the ratio of fracture energy which can vary from ~ 0 when the interface is very weak to 1, when the interface is indistinguishable from the granule. When the interface is weak, intergranular fracture would be expected to dominate. When the interface is well cohered at high compaction pressure, more transgranular fracture would be expected resulting in a

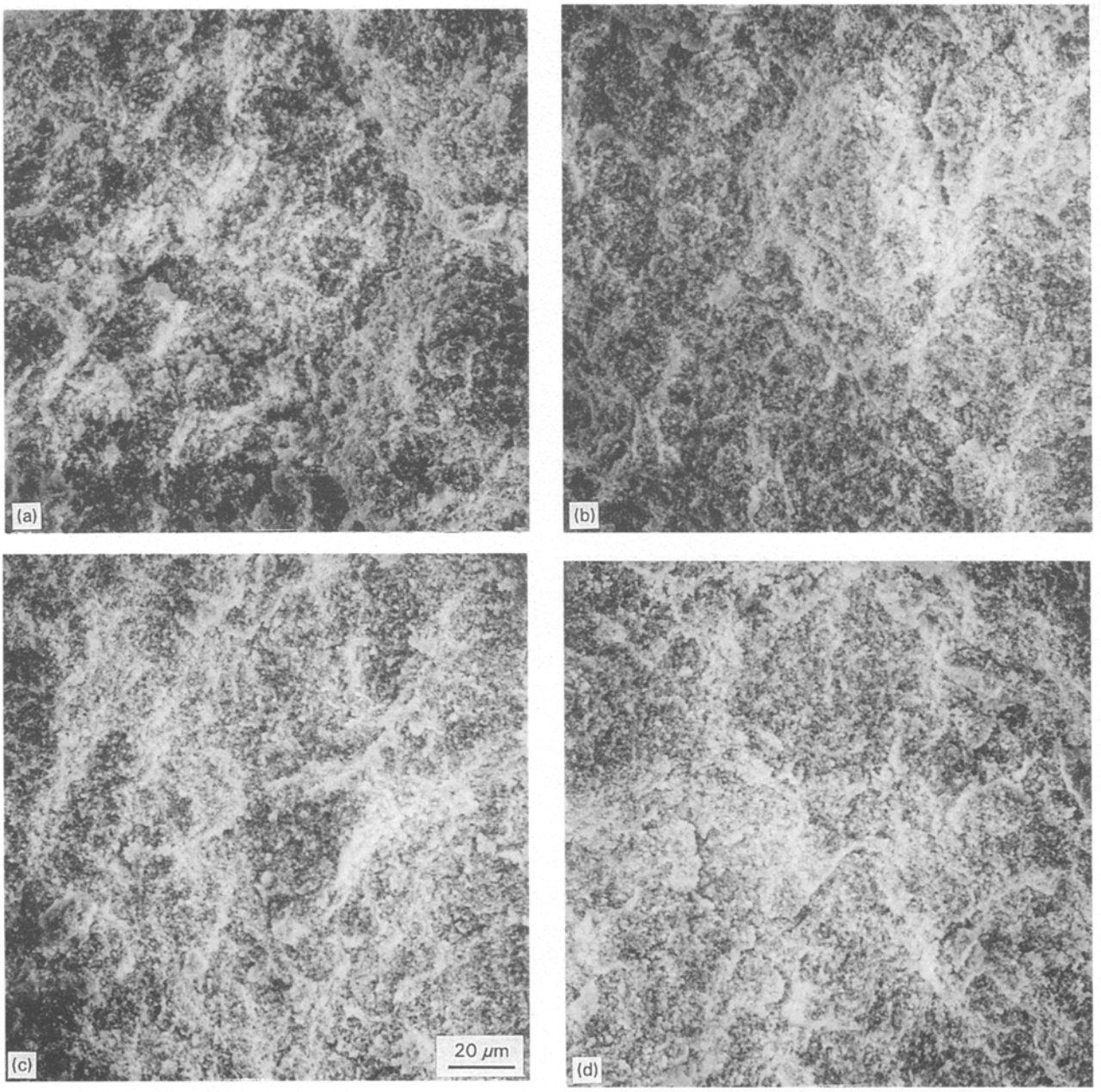

Figure 13 SEM fracture surface of soft granules compacted at (a) 100 MPa; (b) 200 MPa; (c) 300 MPa; and (d) 400 MPa. Fracture surface is transgranular from low to high pressure, suggesting good lamination between granules at low pressure.

correspondingly higher overall material toughness for the pressed bars.

Scanning electron (SEM) micrographs of fracture surfaces of bars compacted at 100 to 400 MPa are shown in Fig. 12(a–d) for the strong granule systems. The fracture surface at 100 MPa exhibited observably more intergranular fracture while the 400 MPa samples exhibited more transgranular fracture. The change in fracture behaviour indicates that the granular interface had been strengthened. Higher fracture toughness and the corresponding increase in strength are evidently associated with an improved intergranular cohesion at high compaction pressure. Similar changes in fracture surfaces as a function of compaction pressure can also be observed in other compacts of spray dried alumina granules [11] and barium titanate granules [12]. Intergranular cohesion strengthening can also be effected by increasing the compaction temperature as shown by Nies and Messing [13].

In the case of weak granules where granules are already well cohered at 100 MPa, fracture surfaces showed similar transgranular fracture irrespective of compaction pressure (Fig. 13), which is consistent with the observed marginal increase in fracture toughness and green strength for bars from weak granules (Figs 5 and 8).

5. Remarks

Strength for composite particulate bodies made from polymer and powder had been reported to follow Griffith's relation [14–17], in that the strength is inversely related to the root of the critical flaw size. For the pressed bars investigated in the present study, the presumed critical flaws are the intergranular voids

and boundaries. Their effective sizes as calculated from peak strength should decrease with increasing pressure as intergranular contact areas are improved at high compaction pressure. Contrarily, experimental data and analyses indicated that the effective flaw size is independent of the compaction pressure, i.e. independent of the decrease in the size of the processing flaw. This discrepancy can be explained by considering the response of the pressed granular microstructure under bending.

In a pressed granular microstructure, intergranular boundaries and voids at triangular junctions are stress concentrations at which deformation would initiate. Under bending, intergranular boundaries will open forming microcracks *throughout* the tensile portion of the bar resulting in an increase in compliance (Fig. 3). Upon further loading, the microcracks would coalesce into a major crack which would lead to final failure of the bar. The effective flaw size calculated from the peak strength is therefore not the initial flaw size associated with the processing and the compaction pressure, but is associated with the critical flaw formed by coalescence of the microcracks. Consequently, the effective flaw size calculated from peak load is not a function of the compaction pressure as is observed in the present study. The relation between microcrack formation and processing parameters will be addressed in future work.

6. Summary and Conclusion

The mechanical properties of green ceramic bodies compacted from granules had been investigated. Because of the non-linear behaviour of the load–displacement curve, data analysis accounting for the non-linearity had been developed to analyse the strength. In addition to strength, the elastic modulus, the fracture toughness and effective flaw size were determined from experimental data as a function of pressing pressure and relative density. The elastic modulus, strength and toughness had been found to increase as a function of compaction pressure and relative density, but the effective flaw size was found to be independent of compaction pressure and relative density. Microstructural examination of the fracture surface revealed that the samples which exhibited an increase in fracture toughness had an increased faction of high energy transgranular fracture owing to improved intergranular cohesion at high compaction pressure. High strength in green bodies compacted at high pressing pressure is primarily attributable to improved cohesion between granules.

References

1. L. M. SHEPPARD, *Bull. Amer. Ceram. Soc.* **72** (1993) 28.
2. S. P. TIMOSHENKO and G. M. GERE "Mechanics of materials" (Van Nostrand Reinhold, New York, 1972) p. 288.
3. JIS R-1601 and JIS R-1602, Japan Industrial Standards, (Japan Industrial Standards Association **36** 1991) p. 252 and p. 254.
4. D. BROEK "Elementary engineering fracture mechanics," 4th Edn (Martinus Nijhoff, New York, 1986) p. 201.
5. E. KLAR and W. M. SHAFER, in "Modern developments in powder metallurgy," **9**, edited by W. Leszynski (Metal Powder Industries Federation, Princeton, New Jersey, 1976) p. 91.
6. K. E. EASTERLING and A. R. THÖLÉN, *Powder Metall.* **16** (1973) 112.
7. E. KLAR and W. M. SHAFER, *Int. J. Powder Metall.* **5** (1969) 5, and **5** (1969) 5.
8. J. A. LUND, *Int. J. Powder Technol.* **18** (1982) 117.
9. A. G. EVANS, B. J. DALGLEISH, M. HE and J.W. HUTCHINSON, *Acta Metall. Mater.* **37** (1989) 3249.
10. A. G. EVANS and B. J. DALGLEISH, *Ibid.* **40** (Supplement) (1992) S-295.
11. R. A. DIMILIA and J. S. REED, *Bull. Amer. Ceram. Soc.* **62** (1989) 484.
12. J. A. BREWER, R. H. MOORE, and J. S. REED, *Ibid.* **60** (1981) 212.
13. C. W. NIES and G. L. MESSING, *J. Amer. Ceram. Soc.* **67** (1984) 301.
14. M. ABDEL-GHANI, J. G. PETRIE, J. P. K. SEVILLE, R. CLIFT and M. J. ADAMS, *Powder Technol.* **68** (1991) 113.
15. M. J. ADAMS, *J. Powder. Bulk Sol. Technol.* **9** (1985) 15.
16. M.A. MULLIER, J. P. K. SEVILLE, M. J. ADAMS, *Powder Technol.* **65** (1991) 321.
17. *Idem., Chem. Eng. Sci.* **42** (1987) 667.

Received 4 July 1994
and accepted 11 May 1995